

Instrumentally induced spurious polarization of a multi-layer half wave plate for a CMB polarization observation

Hiroaki Imada^{1,2,*}, Tomotake Matsumura³, Ryota Takaku⁴, Guillaume Patanchon⁵, Hirokazu Ishino⁶, Yuki Sakurai³, Kunimoto Komatsu⁶, Nobuhiko Katayama³

¹*Institute of Space and Astronautical Science (ISAS), Japan Aerospace Exploration Agency (JAXA), 3-1-1 Yoshinodai, Chuo-ku, Sagami-hara, Kanagawa, 252-5210, Japan*

²*Laboratoire de l'Accélérateur Linéaire, Université Paris-Sud, CNRS/IN2P3, Université Paris-Saclay, Université Paris-Sud, Bâtiment 200, 91898 Orsay, France*

³*Kavli Institute for the Physics and Mathematics of the Universe (Kavli IPMU), The University of Tokyo Institutes for Advanced Study (UTIAS), The University of Tokyo, Kashiwa, Japan*

⁴*Graduate school of Science, The University of Tokyo, Tokyo, Japan*

⁵*Paris Diderot University, Paris, France*

⁶*Okayama University, Okayama, Japan*

*Contact: imada@lal.in2p3.fr

Abstract—Recent cosmic microwave background (CMB) polarization experiments employ a rotating half wave plate (HWP) as a polarization modulator. In order to cover a wide range of a radio frequency, a multi-layer HWP has been studied. In this paper, we set up a numerical model of a 9-layer HWP based on the design for LiteBIRD and estimated the optical properties. Sub-wavelength structure for anti-reflection was also modeled. We used a commercial software based on Rigorous Coupled-Wave Analysis. We have confirmed that spurious polarization by a HWP does not appear for a normal incidence. On the other hand, the spurious polarization can be observed for an oblique incidence. When the incident angle is 10 degrees the magnitude of the spurious polarization is about 10^{-4} , which is comparable to the effect of the gravitational lensing B-mode. We have also confirmed that this design has the potential to achieve a highly efficient polarization modulator.

I. INTRODUCTION

Many inflation theories predict that the evidence of inflation should appear in the cosmic microwave background (CMB) B-mode polarization pattern. Various CMB polarization experiments to search for the B-mode polarization pattern are proposed and some of them have started to observe CMB [1-7]. CMB B-mode polarization is so weak that it is hard to detect the signal. Therefore, recent CMB polarization experiments require three things: a field of view to be sufficiently wide to arrange many detectors on a focal plane, observing bands to be sufficiently broad to remove the effect of foreground sources, and a rotating half wave plate (HWP) to modulate the CMB polarization. If we modulate the signals with a rotating HWP, it is not necessary to take a difference between two detector outputs by adjusting different gains. In addition, a HWP can save the weak signals from $1/f$ noise by shifting them to the higher frequency.

A HWP accurately makes a phase retardation of π radians at a specific wavelength. When a HWP is employed to CMB experiments, the polarization properties of a HWP should be independent of wavelengths and incident angles. An achromatic HWP can be achieved by combining several HWPs but the polarization properties of a HWP vary as a function of the incident angle [8-11]. In the point of view of a CMB polarization experiment, the leakage from unpolarized light to linear polarization, hereafter I-to-P leakage, can contaminate the CMB polarization map.

In this paper, a HWP is assumed to be one that is designed for the Low Frequency Telescope (LFT) on the LiteBIRD [1], a next generation CMB polarization satellite. The HWP for LiteBIRD will be composed of 9 sapphire plates [12] and equipped with a sub-wavelength structure for anti-reflection. We summarize the characterization of a HWP with the Mueller matrix from the point of view of a CMB experiment in Section II. In order to calculate all the Mueller matrix elements as a function of frequency and incident angle, we set up a model for the numerical simulation in Section III. Section IV shows the simulation results and an I-to-P leakage in the results can be found. Finally, we discuss the causes of the I-to-P leakage and whether or not the amount of I-to-P leakage can be acceptable for LiteBIRD.

II. CHARACTERIZATION OF HWP

Mueller matrix [13] is one of useful tools to express the character of a polarizing optical element. When we introduce the angle of an optic axis, ρ , with respect to the direction along which a detector is sensitive to light polarized (Fig. 1), an ideal HWP can be expressed as

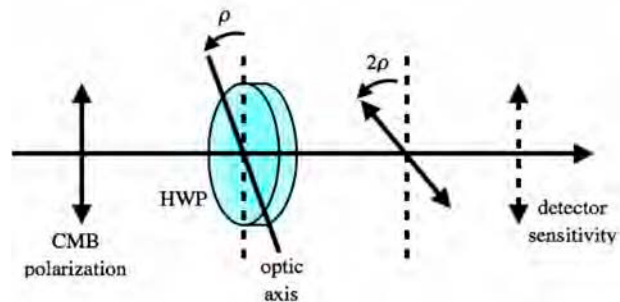


Fig. 1. A diagram showing then incident CMB polarization, HWP optic axis, and detector sensitivity.

If we employ a polarized detector sensitive to the Stokes parameter $Q > 0$, i.e. linear polarization, the ideal HWP allows us to detect CMB polarization at a frequency of 4ρ as follows:

When we consider a more realistic case, each element of the Mueller matrix can have a non-zero component at a frequency of 4ρ due to the combination of fresnel reflection, oblique incidence, and so on. Therefore, it is assumed, in general, that the Mueller matrix should be written with the summation of Fourier harmonics of the HWP rotation angle of ρ as

where X , and Y represent I , Q , U , and V , θ is an incident angle to a HWP, and Φ is an azimuthal angle. Using A_{XY} , C_{XY} , and $\varphi^{(4)XY}$, We can define a modulation efficiency η , for example, as

Since modulated CMB signals appear at a frequency of 4ρ , it is useful to focus on what effects each coefficient C_{XY} provides on the output signals.

We can categorize C_{XY} into 4 groups. First group contains C_{QQ} , C_{QU} , C_{UQ} , and C_{UU} . They are unity for the ideal HWP case and determine the modulation efficiency η and polarization angle through $\varphi^{(4)QQ}$, $\varphi^{(4)QU}$, $\varphi^{(4)UQ}$ and $\varphi^{(4)UU}$ for a general HWP case. Second group contains C_{II} , C_{VI} , C_{VQ} , and C_{VU} . They cause the modulation efficiency to decrease because they convert light to circular polarization that is identified as a constant signal independent of the rotation angle ρ for a linear polarized detector. C_{IV} , C_{QV} , C_{UV} , and C_{VV} are sorted into third group.

They can be ignored as long as CMB and astronomical sources have Stokes V equal to zero. The last group, which is most important in terms of spurious signal, has C_{IQ} , C_{IU} , C_{QI} , and C_{UI} . They cause spurious polarization from unpolarized light. They should be 10^{-4} or less from our study. When the magnitude of C_{IQ} , C_{IU} , C_{QI} , and C_{UI} are 10^{-4} , we estimate that the contamination from unpolarized light has an effect on the polarimetry of CMB signal, which is comparable to the gravitational lensing effect. Table 1 summarizes the four groups.

III. SIMULATION

The HWP for the LiteBIRD LFT will be made of 9 sapphire plates with each thickness of 3.14mm. The refractive indices for ordinary and extraordinary rays are assumed to be 3.047 and 3.361, respectively. No dielectric loss is assumed. The optic axes are arranged at 18.5, 37.5, 73.9, 141.5, 73.9, 37.5, 18.5, 22.7 degrees with respect to the first plate. The first and ninth plates are equipped with sub-wavelength structure for antireflection (Fig. 2). The pitch is $300 \mu\text{m}$, height $2000 \mu\text{m}$, tip $20 \mu\text{m}$, and bottom $20 \mu\text{m}$.

The polarization state of an incident plane wave for this simulation is assumed to be linear. The frequencies for simulation are 119 GHz, 161 GHz, and every 5 GHz from 125 GHz to 155 GHz. This frequency range corresponds to the 140 GHz band for LiteBIRD. The incident angles to a HWP are 0 and 10 degrees, which corresponds to the maximum angle of LiteBIRD LFT optical design. Note that the normal incident case was calculated only at 140 GHz.

In order to simulate our HWP model including the sub-wavelength structure, we used DiffractMOD [14] based on Rigorous Coupled-Wave Analysis (RCWA) [15]. Since RCWA is an algorithm dedicated to a periodic structure, RCWA is suitable for calculating the electromagnetic field of the complicated but periodic structure as shown in Fig. 2.

The computer resources we used for this analysis were a CPU operating at 2.6 GHz with 14 threads, RAM with about 110 GB. It took 30 hours for a Mueller matrix at a specific frequency for a normal incidence and 60 hours for an oblique incidence.

TABLE I
CATEGORIZING C_{XY} .

group	Coefficients	Effect on Polarimetry
1	$C_{QQ}, C_{QU}, C_{UQ}, C_{UU}$	modulation efficiency and polarization angle
2	$C_{II}, C_{VI}, C_{VQ}, C_{VU}$	reducing modulation efficiency
3	$C_{IV}, C_{QV}, C_{UV}, C_{VV}$	ignorable
4	$C_{IQ}, C_{QI}, C_{IU}, C_{UI}$	spurious polarization from unpolarized light

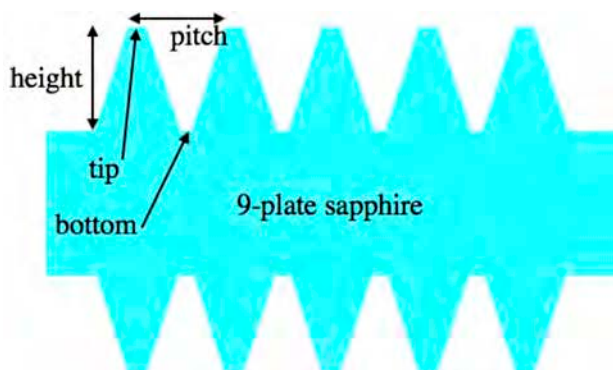


Fig. 2. HWP model with sub-wavelength structure for antireflection.

IV. RESULTS AND DISCUSSIONS

This section shows the simulation results of the normal incident case at 140 GHz, the results of the oblique incident case at 140 GHz, and, in addition, the results of the oblique incident case as a function of frequency.

A. Normal incident simulation at 140 GHz

Fig. 3 shows each element of Mueller matrix as a function of the HWP rotation angle ρ for the normal incidence at 140 GHz. The $4-\rho$ terms can be found only in M_{QQ} , M_{QU} , M_{UQ} , and M_{UU} (cf. group 1 in Table 1). Therefore, spurious polarization does not appear in this case. M_{IQ} , M_{IU} , M_{QI} , and M_{UI} behave as a $2-\rho$ term with an amplitude of about 10^{-3} . This is because Fresnel reflection differ between two polarization states. The $2-\rho$ terms in M_{QV} , M_{IV} , M_{QI} , and M_{UI} comes from the difference of retardation between two polarization states from π radians. The $2-\rho$ terms in M_{IV} and M_{VI} also attribute to the retardation different from π radians as well as the difference of Fresnel reflection between two polarization states at the same time.

B. Oblique incident simulation at 140 GHz

When an incident wave enters obliquely to a HWP, the refractive index for an extraordinary ray depends on the angle between the optic axis and the normal to the incident plane, i.e. $\rho - \Phi$. It is given by ([16])

where n_{inc} is the refractive index in the incident space. The refractive index $n'_e(\Theta, \rho - \Phi)$ itself has $4-\rho$ dependence, which causes Fresnel reflection, refraction angle, and optical path lengths to have additional $2-\rho$ or $4-\rho$ dependence.

Fig. 4 shows the Mueller matrix elements as a function of the HWP rotation angle ρ for the 10-deg. incident case at 140 GHz. We can find the features of a $4-\rho$ element in the other elements as well as M_{QQ} , M_{QU} , M_{UQ} , and M_{UU} . The elements M_{IQ} , M_{IU} , M_{QI} , and M_{UI} have $4-\rho$ terms and higher order terms, which induces spurious polarization. They come from the combination of the difference of Fresnel reflection between two polarization states and ρ -dependence of the index $n'_e(\Theta, \rho - \Phi)$. Their amplitudes are about 10^{-3} . The other elements, M_{QV} , M_{UV} ,

M_{VQ} , M_{VU} , M_{IV} , and M_{VI} , also have $4-\rho$ and higher terms due to the difference of retardation from π radians and the ρ -dependence of refraction angle in addition to the ρ -dependence of Fresnel reflection and the index $n'_e(\Theta, \rho - \Phi)$. Their amplitudes are from 10^{-4} to 10^{-2} .

C. Coefficients A_{XY} , B_{XY} , and C_{XY}

Figs. 5-7 show the amplitudes of each harmonics for 10-deg. incident case. Since Figs. 5-7 are given as a function of frequency, they include the 140-GHz case shown in the previous subsection.

Using on A_{XY} , C_{XQ} , and $\varphi^{(4)}_{XQ}$, we obtain the modulation efficiency of 99.98% at 140 GHz. Fig. 8 shows the modulation efficiency η as a function of frequency. This result indicates that we can achieve an extremely high modulation efficiency of more than 99% with this multi-layer HWP design.

In terms of polarimetry, we should focus on coefficients C_{XY} , especially C_{IQ} , C_{IU} , C_{QI} , and C_{UI} which are closely related to spurious polarization. We can find their amplitudes are about 10^{-4} . Comparing C_{IQ} and C_{IU} , the phases are different by about $\pi/2$ radians. The effect of this magnitude of 10^{-4} is estimated to be comparable to that of the B-mode signal by the gravitational lensing effect. The spurious signal level is not harmful to the systematic error of measuring the CMB polarization. However, further study is needed because detectors has a sensitivity over a wide frequency range and we have to calculate a band-averaged properties such as a modulation efficiency and spurious polarization.

V. CONCLUSIONS

Many CMB polarization experiments start to employ a HWP and some experiments have already observed CMB polarization with a HWP. LiteBIRD, a next generation CMB polarization satellite, also has a plan to employ a HWP as a polarization modulator.

We have characterized the properties of a HWP by using a Mueller matrix and decomposing each element of the Mueller matrix into Fourier harmonics. In terms of polarimetry, the harmonics we should focus on is the 4 times higher frequency term than the HWP rotation frequency, $4-\rho$ term.

We have carried out the numerical simulation to estimate a Mueller matrix of the HWP which is based on the design for the LiteBIRD LFT. The HWP model is composed of 9 sapphire plate and sub-wavelength structure for antireflection on the first and last plate. We used DiffractMOD, commercial software, based on RCWA due to the sub-wavelength structure. The incident wave was assumed to be linear polarized plane wave. The incident angle is 0 degrees for 140 GHz and 10 degrees for 119 GHz to 161 GHz, which corresponds to the LiteBIRD 140 GHz band.

We have confirmed that there is no additional $4-\rho$ term for the normal incident case. On the other hand, for 10-degree incident

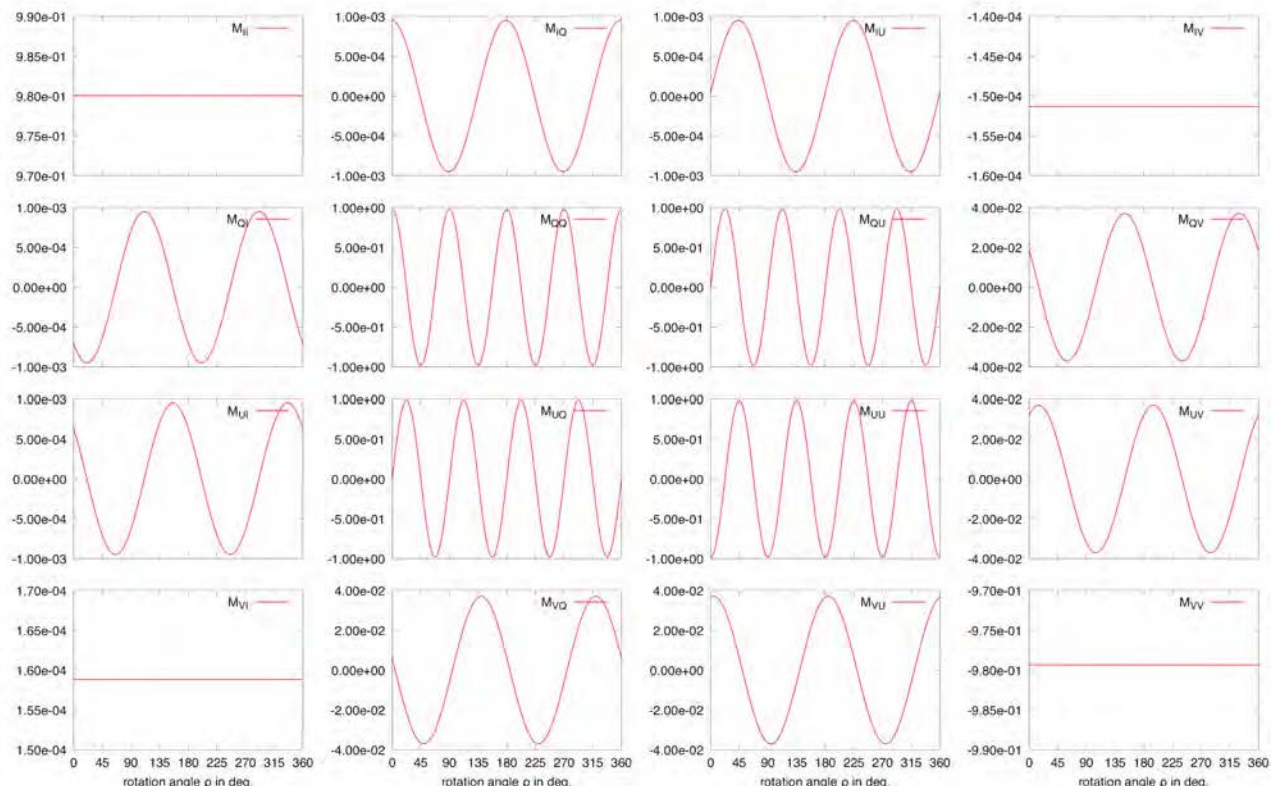


Fig. 3. Mueller matrix as a function of the rotation angle of a HWP, ρ . The results are obtained for the normal incidence at 140 GHz

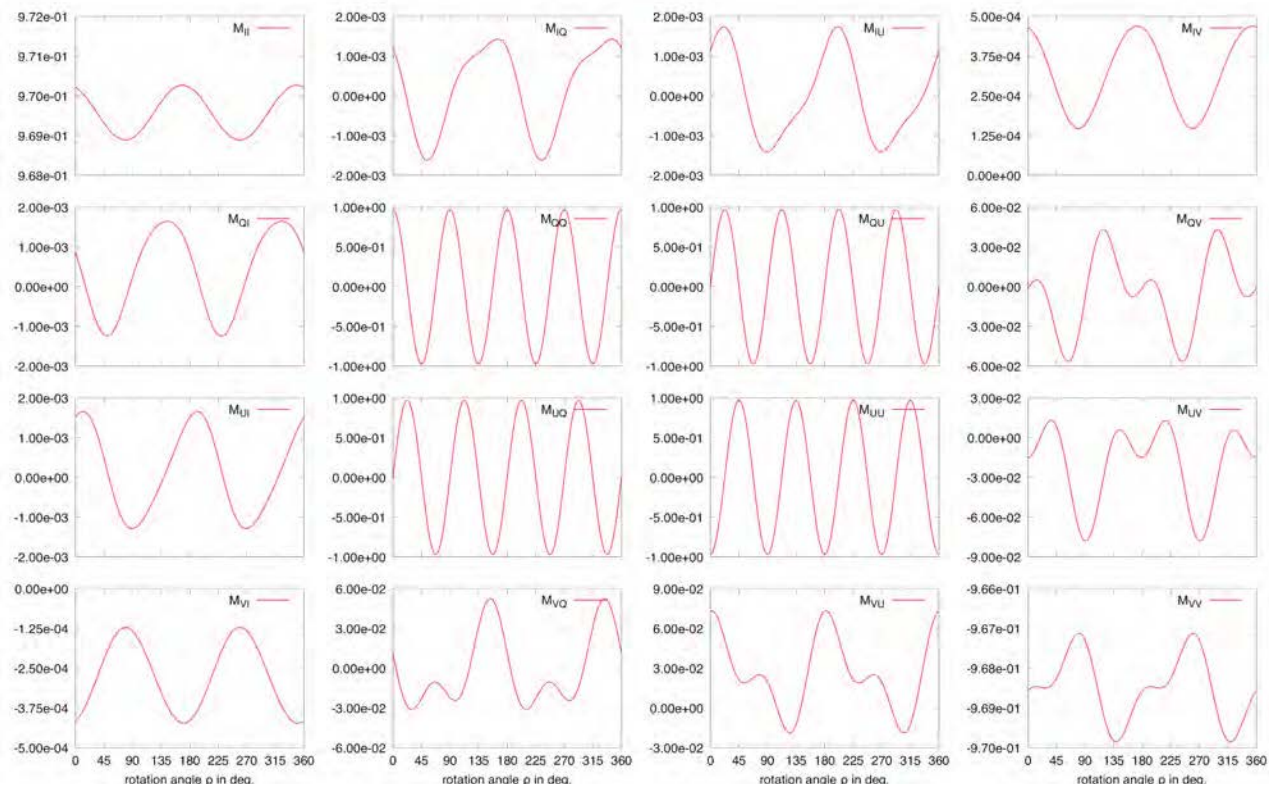


Fig. 4. Mueller matrix as a function of the rotation angle of a HWP, ρ . The results are obtained for the 10-deg. incidence at 140 GHz.

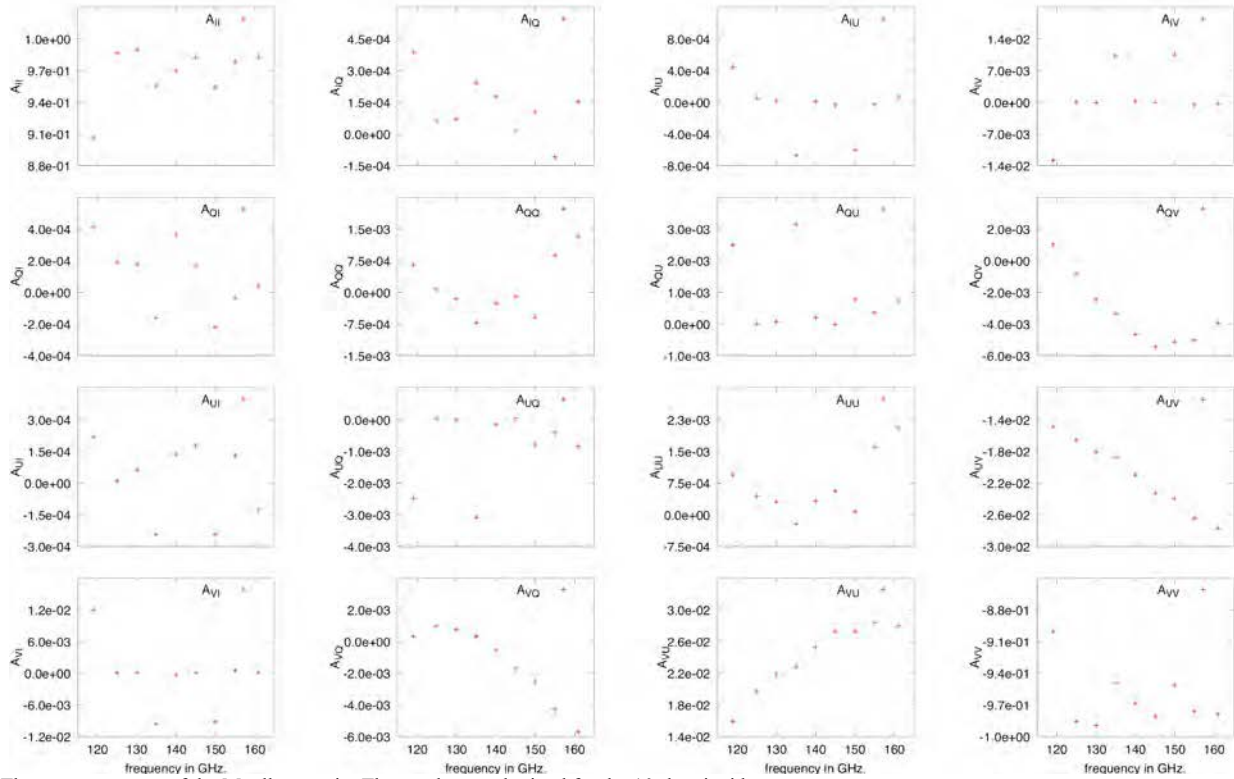


Fig. 5. The constant terms of the Mueller matrix. The results are obtained for the 10-deg. incidence.

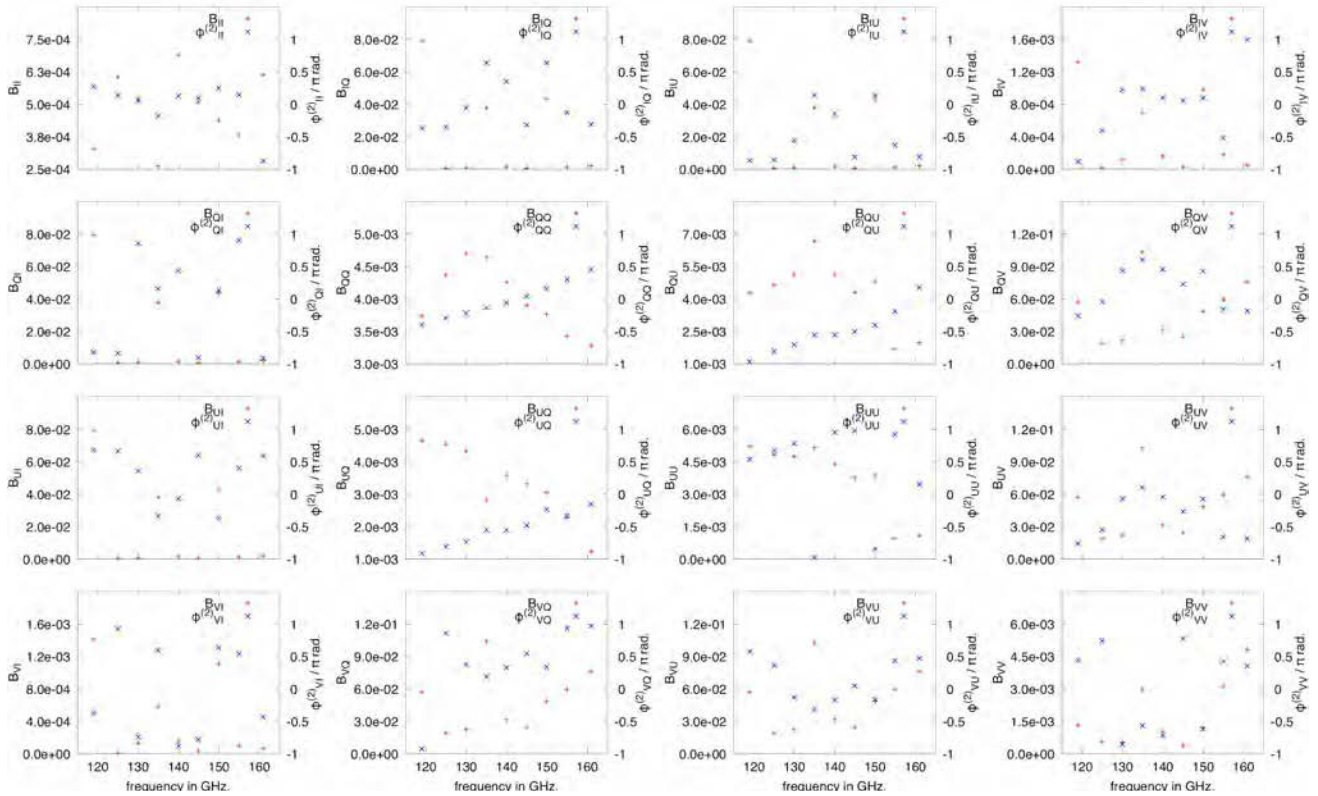


Fig. 6. The $2\text{-}\pi$ terms of the Mueller matrix. The results are obtained for the 10-deg. incidence.

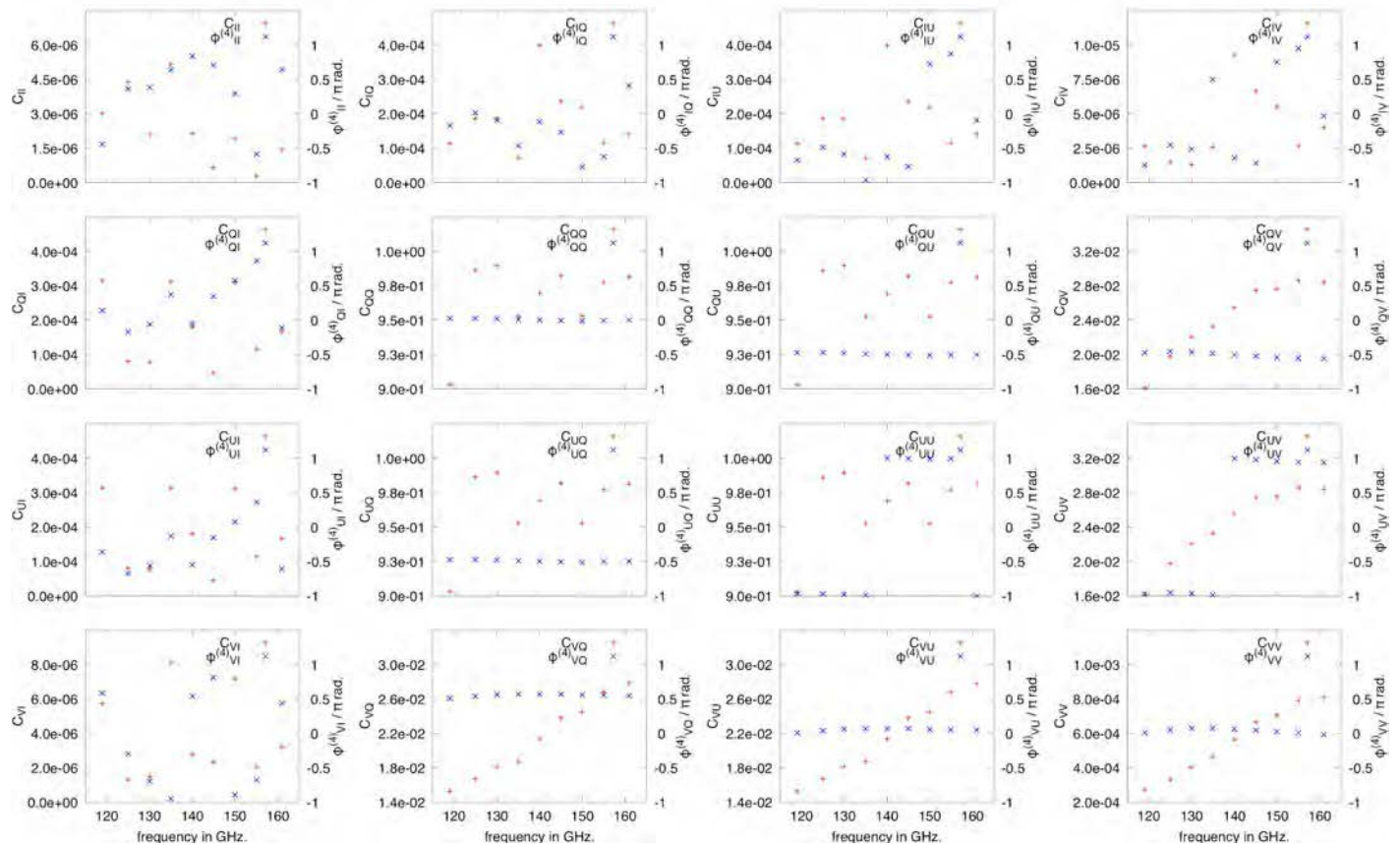
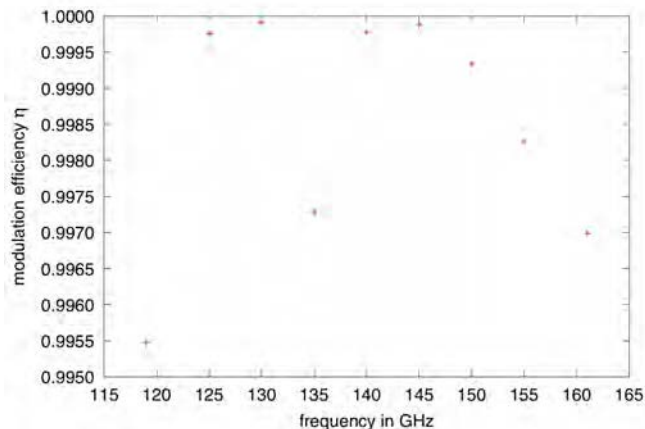

 Fig. 7. The $4\text{-}\rho$ terms of the Mueller matrix. The results are obtained for the 10-deg. incidence.


Fig. 8. Modulation efficiency as a function of frequency.

case, $4\text{-}\rho$ term can be observed, which causes spurious polarization. The spurious polarization attributes to the ρ -dependence of the refractive index of an extraordinary ray. The magnitude of $4\text{-}\rho$ terms relating to the spurious polarization is about 10^{-4} . The effect of this spurious polarization is estimated to be comparable to that of the gravitational lensing B-mode polarization. It is not harmful but further study is needed. We have also confirmed the modulation efficiency is high enough to observe CMB

polarization. This design has the potential to achieve a highly efficient polarization modulator.

ACKNOWLEDGMENT

This work was supported by JSPS KAKENHI Grant Number 15H05891 and 15H05441.

REFERENCES

- [1] H. Ishino, Y. Akiba, K. Arnold, *et al.*, "LiteBIRD: Lite satellite for the study of B-mode polarization and Inflation from cosmic microwave background Radiation Detection," in *Proceedings of SPIE Astronomical Telescopes + Instrumentation*, 99040X, 2016.
- [2] J. Delabrouille, *et al.* "Exploring Cosmic Origins with CORE: Survey requirements and mission design." *Journal of Cosmology and Astroparticle Physics*, 2018.04:014, 2018.
- [3] P. A. R. Ade, Z. Ahmed, R. W. Aikin, *et al.*, "Improved constraints on cosmology and foregrounds from BICEP2 and Keck array cosmic microwave background data with inclusion of 95 GHz band," *Phys. Rev. Lett.*, 116, 031302, 2016.
- [4] P. A. R. Ade, *et al.*, "A Measurement of the Cosmic Microwave Background B-mode Polarization Power Spectrum at Subdegree Scales from Two Years of POLARBEAR Data," *The Astrophysical Journal*, 848.2:121, 2017.
- [5] T. Louis, *et al.*, "The Atacama Cosmology Telescope: two-season ACTPol spectra and parameters," *Journal of Cosmology and Astroparticle Physics* 2017.06:031, 2017.
- [6] A. Kusaka, *et al.*, "Results from the Atacama B-mode Search (ABS) Experiment," *arXiv preprint arXiv:1801.01218*, 2018.

- [7] G. Simard, *et al.*, "Constraints on Cosmological Parameters from the Angular Power Spectrum of a Combined 2500 deg² SPT-SZ and Planck Gravitational Lensing Map," *The Astrophysical Journal*, 860.2:137, 2018.
- [8] S. Pancharatnam, "Achromatic combinations of birefringent plates Part I. An Achromatic Circular polarizer," in *Proceedings of the Indian Academy of Sciences*, vol. XLI, no. 4, sec. A, pp. 130-136, 1955.
- [9] C. J. Koester, "Achromatic Combinations of Half-Wave Plates," *JOSA*, 49, 4, pp. 405-409, 1959.
- [10] G. Pisano, *et al.*, "Achromatic half-wave plate for submillimeter instruments in cosmic microwave background astronomy: experimental characterization," *Applied Optics*, 45, 27, pp. 6982-6989, 2006.
- [11] T. Matsumura, *et al.*, "Performance of three- and five-stack achromatic half-wave plates at millimeter wavelengths," *Applied Optics*, 48, 19, pp. 3614-3625, 2009.
- [12] K. Komatsu, *et al.*, "Prototype design and evaluation of the nine-layer achromatic half-wave plate for the LiteBIRD low frequency telescope," in *Proceedings of SPIE Astronomical Telescopes + Instrumentation*, in press., 2018.
- [13] E. Hecht, *Optics Fifth edition*, Edinburgh: Pearson Education Limited, 2017.
- [14] *RSoft DiffractMOD v2017.03 User Guide*, Synopsys, Inc., 2017.
- [15] M. G. Moharam, T. K. Gaylord, "Rigorous coupled-wave analysis of metallic surface-relief gratings," *J. Opt. Soc. Am. A* 3, 1780, 1986.
- [16] S. Orfanidis, *Electromagnetic Waves and Antennas*, S. Orfanidis, 2016.